3. 1. 2. 4 DTL, SDTL

Construction started on the Alvarez-type DTL and the separated DTL (SDTL) according to the design for the JHP project [1,2], to accelerate H^- ions from 3 to 200 MeV. The DTL consists of three long tanks (maximum 9.9 m in length), each of which is comprised of three short unit tanks (approx. 3 m in length), to overcome difficulties in constructing the tank and assembling the drift tube. Furthermore the SDTL consists of 32 short tanks of which the length varies from 1.5 m to 2.5 m. The resonance frequency of the DTL and SDTL is 324 MHz.

3. 1. 2. 4. 1 Rf and mechanical features of the DTL and SDTL tanks

The most important required property for the DTL and SDTL accelerator complex is that they show stable performance during a long operation period with a long pulse length and a high duty factor. Also, it is necessary to suppress any deviation of the operation condition from the design values to be as small as possible in order to achieve well-controlled operation based on a comparison between the measured beam properties and the calculated one. We adopt the following strategy for satisfying the requirements:

1. The advanced process of copper electroforming by periodic reverse (PR) electrolysis for producing the lining is utilized to make all of the inner surfaces of the tanks for suppressing the discharge issues [3,4,5].
2. The pulsed focusing magnet system for the DTL is adopted for decreasing the heat dissipation from the magnets in the drift tubes. Thus, a more stable field distribution in a DTL tank, which differs little from the low-level field measurements, during high-power operation can be expected.
3. The field in the DTL is stabilized by post couplers.
4. The requirements for the mechanical accuracy for fabrication and alignment of each components are sufficiently high.
5. The requirements for the stability of power supply of both the rf sources and magnets and water-cooling system are sufficiently high.

Important spects of the DTL construction, which have been developed in order to achieve the requirement described above, are described in the following section.

3. 1. 2. 4. 2 RF contactor

An rf contactor is one of the most important components for rf cavity construction, because the DTL uses many contactors for assembling each component of the tank, and then the performance of the contactor fixes the total rf properties of the tanks [6].

Two types of rf contactors have been developed: (a) a contactor between the end plate and the tank cylinder; and (b) a contactor between the stem of the drift tube and the tank. Cross-sectional views of the contactors are shown in Figure 3.1.2.4.1. The structure is very simple: a thin copper layer (0.5 mm in thickness) surrounds a stainless-steel spring. There is a vacuum seal outside the rf contactor. The performance of these was checked initially by a small test tank and then by the large tanks described in the next section.

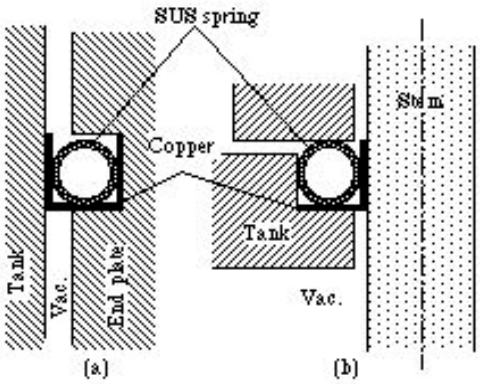

Figure 3.4.2.4.1 rf-contactors

(a) rf-contactor between the end-plate and the tank, (b) rf-contactor between the stem of the drift tube and the tank.

3. 1. 2. 4. 3 Vacuum and rf properties of the test tank

The cylindical tank of the DTL is made of iron, with the inner surface covered by a copper layer (0.5 mm in thickness) that was built by the Periodic Reverse (PR) electroforming using a pure copper sulphate bath, and then finished by electropolishing [3,4,5]. A cylindrical cavity was made to test the vacuum and the rf properties of the PR copper electroforming surface. The size of the cylinder (560 mm in diameter, 3320 mm in length) is almost identical to that of the longest unit tank of the DTL. The rf contactor described in the previous section is used for end plates.

The measured unloaded Q-value of the TM010 mode of the cavity is 77000, which represents approximately 97% of the value obtained by analytical calculations. The results indicate that (a) the electrical quality of the copper surface is sufficiently high

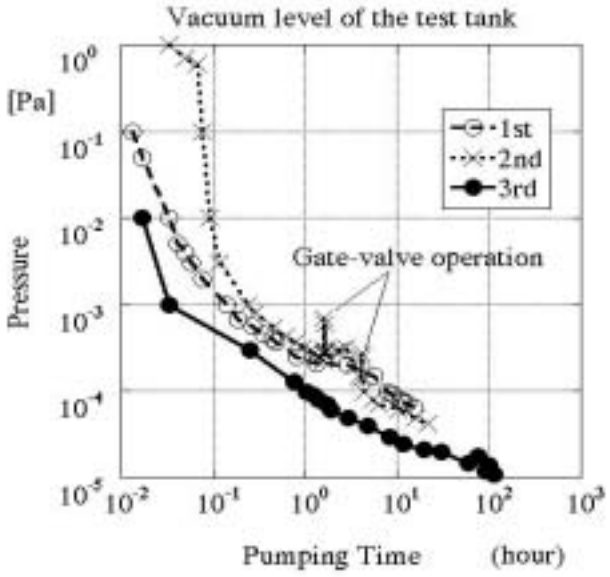

Figure 3.1.2.4.2.

Ultimate pressure for the 3m tank.

and (b) that the rf contactor functions satisfactorily at a low rf-power level.

The vacuum property was also measured and, as the results in Figure 3.1.2.4.2 show, the pressure level of the tank became 10^{-5} Pa after 100 hours of evacuation. The outgas rate from the tank surface was also measured by an integration method (build-up test) and the data is presented in Figure 3.1.2.4.3. The outgas rate for the 2nd measurement was 5.2×10^{-8} Pa $m^3/s/m^2$ (3.9×10^{-11} Torr $l/s/cm^2$), which is closely consistent with the value for the OFC.

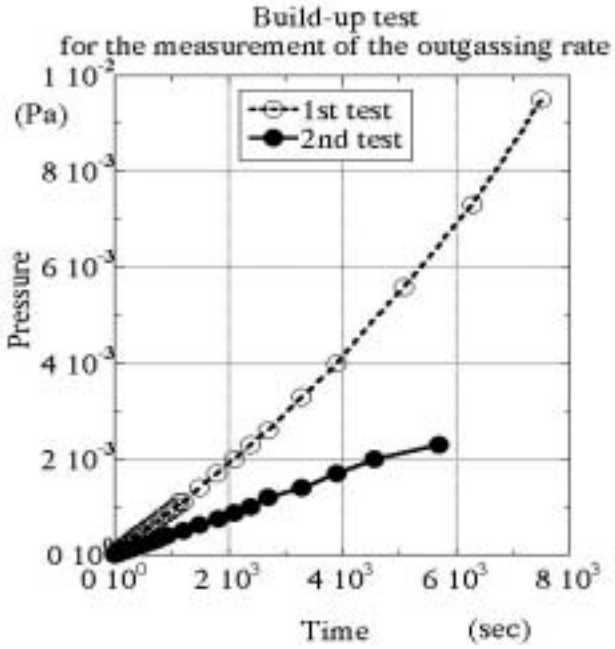

Figure 3.1.2.4.3.
Pressure variation in the tank with outgasing.

3. 1. 2. 4. 4 Quadrupole magnet for the DTL [7,8]

The quadrupole magnet in the drift tube is also a very important compornent. Beam dynamics require that the magnets and the DTs for the low-energy part of the DTL conform to the following specifications:

1. The magnetic field gradient must be variable.
2. The electromagnet must be installed within the compact DT (outer diameter within 140 mm, length about 52 mm).
3. The magnet must have a sufficiently large bore diameter (nearly 16 mm) and a high magnetic field (an integrated magnetic field gradient is 4.1 Tesla).
4. Expansion of the DT in the beam-axis direction should be less than 10 micro-meter on one side during operation.
5. The deviation of a quadrupole field center from the mechanical center must be within 15 micron-meters.

In order to satisfy these requirements, pulsed electromagnets have been selected, instead of permanent magnets. However, if we use the conventional hollow conductor-type coil, it is very difficult to make an electromagnet which can be installed within a 324-MHz DT, since a rather large bending-radius is necessary for hollow conductors. Consequently, we newly developed an electroformed hollow coil. This new method makes use of an advanced Periodic Reverse (PR) copper electroforming combined together with various kinds of machining processes without welding (except for the connection to the outside of DT), where the outer surfaces of the coil consists of an electroformed copper layer.

Table 3.1.2.4.1. Design parameters of the Q-magnets and the DTs for the low-energy part of the DTL.

Magnet aperture diameter	(mm)	15.6
Core length: L	(mm)	33.0
Integrated field: GL(GLe)	(Tesla)	4.1
Effective length: Le	(mm)	39.2
Core material:	Silicon steel leaves 1)	
Main thickness of leaf	(mm)	0.5
Yoke outer diameter	(mm)	115
Nnumber of turns per pole	(turns/pole)	3.5
Maximum Ampere-Turns	(AT/pole)	3500
Excitation current (Pulse)	(A)	780
Pulse repetition rate	(Hz)	50
Pulse operation	rise time 5 ms, flat top duration 2 ms	
Minimum coil size	(mm)	h 5.5, w 5.3, t 1
Voltage drop	(V)	1.8
Resistance	(mm Ω)	2.3
Inductance	(μH)	18
Water flow rate	(liter/min)	1.0
Water temperature increase	(deg.)	3.0
Water pressure drop	(kg/cm2)	1.8
DT outer diameter	(mm)	140
DT aperture diameter	(mm)	13.0
DT length	(mm)	52.5

Note: 1) Nippon Steel Corporation., type 50H400 [9]

The design parameters of the Q-magnets and the DTs that we developed for the low-energy part of the DTL are listed in Table 3.1.2.4.1.

Figure 3.1.2.4.4 shows a detail of a corner part of the electroformed hollow coil.

The coil manufacturing process is outlined next. After cutting grooves for the water-cooling channel in a copper block (Fig. 3.1.2.4.5 (a)), they are filled with a wax, which is coated with silver powder to achieve electronic conductivity (ibid. (b)).

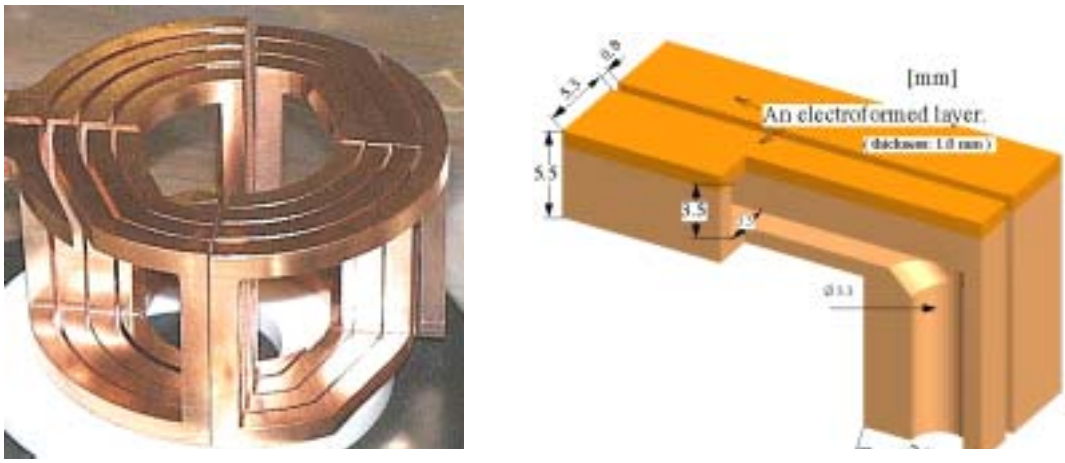

Fig. 3.1.2.4.4.
Detailed illustration of a corner part of the electroformed hollow coil.

A 0.5 mm thick copper layer is formed at each end face by PR copper electroforming (ibid. (c)). After machining the surfaces, additional copper deposits are formed (0.5 mm thickness). After removing the wax and boring the pole-piece part (ibid. (d)), the coils of the end faces are separated using an end mill of 0.8 mm in diameter (ibid.(e)). The coils in the beam-axis direction are then separated to 1.0 mm by a wire-cutting

(a)
Groove processing for the water-cooling channel.

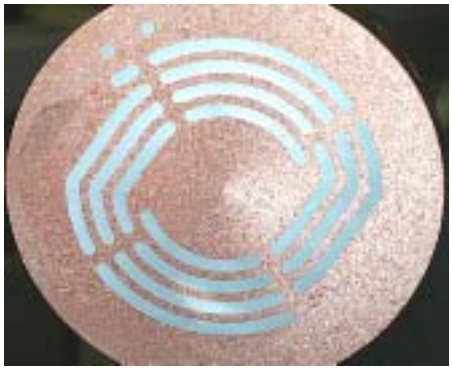

(b)
Filling with silver powder Coated wax.

(c)
PR electroformed surface.

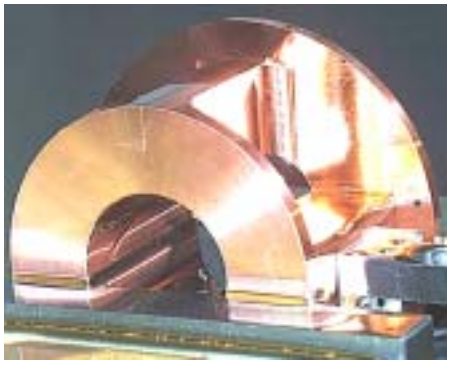

(d)
Cutting of the pole-piece part.

(e)
Separation of the coils by end mill.

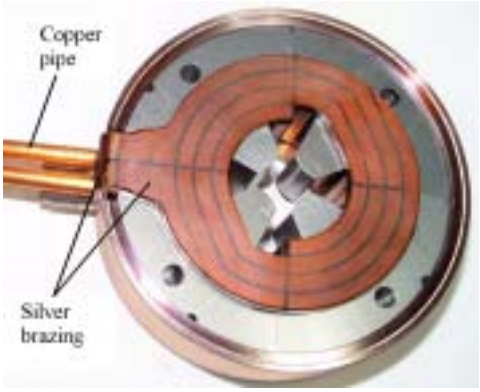

(f)
Silver brazing of magnet leads.

Figure 3.1.2.4.5.
Outline of the manufacturing process for an electroformed hollow coil.

machine (Fig. 3.1.2.4.4). In this way, the coil inside the DT is molded without welding. Finally, the magnet leads are connected to the coils with silver brazing (Fig. 3.1.2.4.5 (f)).

In order to reduce pressure drops and the effects of erosion, the water velocity in the coil is limited to under 2 m/s. For the same reason, a bending corner inside the water-cooling channel is partly cut. As a result, the measured pressure drops are 1.8 and 6.3 kg/cm^2 for the water flows of 1 and 2 Liter/minute, respectively.

Some important properties of the magnets were measured before installing into the DT. Figure 3.1.2.4.6 shows the excitation-current dependences of the field gradients. The measured data are compared with those 3-D analyzed by MAFIA. Both are in agreement within approximately 2%.

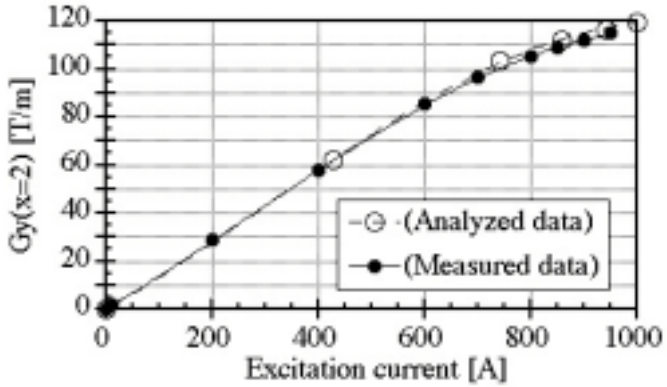

Figure 3.1.2.4.6.
Comparison of excitation-current dependences on the magnetic field gardient for measured data and 3-D analyzed data using MAFIA.

Furthermore, the higher order multipole components in the magnetic field center measured by a rotating coil were sufficiently small, being less than 0.11% compared with the quadrupole component (Fig. 3.1.2.4.7). Also, the field center deviated by only about 4 μm from the mechanical center.

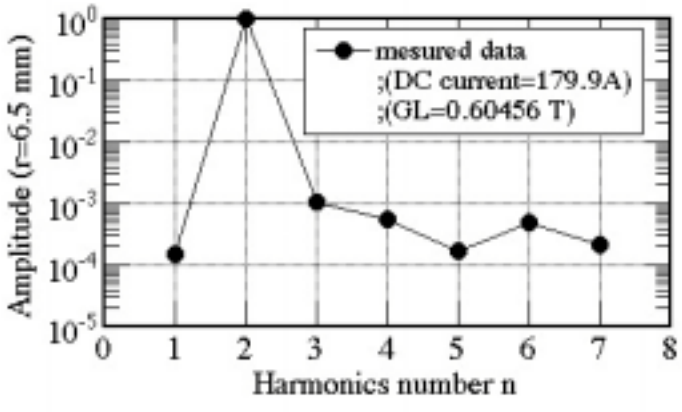

Figure 3.1.2.4.7.
Higher-order multipole components in the center of the magnetic field.

After installing the magnet into the DT, some properties were also measured during field excitation. Figure 3.1.2.4.8 shows the dependence of the water-temperature increase upon the excitation-current. The temperature increase in the coil for water-flow rate of 1 liter/minute and the design excitation-current of 780 A was 3 degrees, which is within the specification range. The drift tube was also water-cooled. However, variations in the flow rate of the DT had no measurable influence on the water-temperature of the coil. This is probably because the heat load on the coil is not very heavy.

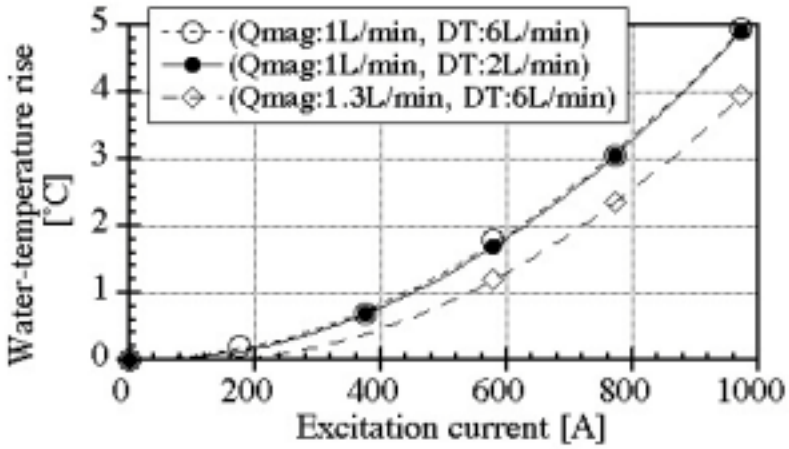

Figure 3.1.2.4.8.
Excitation-current dependences on an increase in the water temperature of the electroformed coil.

The resonant frequency of the test tank, which is 1.4 m in length, was reduced by approximately 220 Hz, when the magnet was excited at the maximum current (for the design water-flow rate). This corresponds to an approximately 0.4 μm expansion of the first drift-tube length.

3. 1. 2. 4. 5 Specification of all the Q-magnets

The specifications of all Q-magnets in the DTL are shown in Table 3.1.2.4.2. Seven kinds of core lengths and five kinds of bore diameters were chosen in order to make a trade-off between the requirements determined from the beam dynamics and a reduction in the fabrication cost. The cross sections of the coils for all of the magnets are equal.

Table 3.1.2.4.2.
Specifications of all the Q-magnets in the DTL. (A unit is mm)

DTL tank No.	1					2		3
Number of the DTs	77					44		28
Qmag outside diameter	115					115		115
Qmag core length	33	35	50	76	80	80	90	125
Qmag bore diameter	15.6	16	16	21	21	25	25	29
Number of the magnets	6	17	33	1	20	1	44	28

3. 1. 2. 4. 6 Quadrupole doublets for the SDTL

We have developed 31 sets of quadrupole doublets for installing among SDTL tanks. All Q-magnets have the same specifications. The bore diameter of the Q-magnets should be chosen to be as large as possible compared with beam diameter in order to avoid beam losses. Here, the calculated maximum beam diameter was about 30 mm in the SDTL, where the alignment error was included. The parameters of the Q-magnets are shown in Table 3.1.2.4.3. In order to measure the transverse beam position and beam width, beam-position monitors (BPM) attached into a short vacuum duct were installed in the bore holes of all Q-magnets. Thus, the shape of pole-tips was carefully designed and fabricated the satisfy the requirements. A cross-sectional view of these magnets is shown in Fig. 3.1.2.4.9.

In order to achieve a magnetic field gradient having a uniform distribution, the shape of the poles was optimized based on two and three-dimensional analyses using POISSON and MAFIA. Figure 3.1.2.4.10 shows the radial distribution of the integrated field with the design current. The integrated field is uniform within 0.2% over the radial region from the beam axis to the aperture radius of a beam duct.

We measured the magnetic field of the quadrupole doublet by using a Hall probe. Figure 3.1.2.4.11 shows the measured longitudinal distribution of the quadrupole doublet, excited at the maximum current by a series connection. When two quadrupole magnets were aligned to each other according to the doublet scheme, some difference in both fringing fields of the magnet was observed; the field in the neighboring magnet side was slightly smaller that in the other side. In this case, the decrease of the integrated field in the fringing field of the neighboring magnet side (-50<Z<50) occupies about 0.5% of the total integrated field. Measurements of the field distribution for all quadrupole magnets using a rotating coil are under way.

Table 3.1.2.4.3. Parameters of the quadrupole doublets for SDTL.

		Q1～Q62
Integrated field: GL	[T]	1.91～2.64
Maximum GL	[T]	3.36
Maximum field: G	[T/m]	30
Effective length	[mm]	112
Core length	[mm]	90
Aperture diameter	[mm]	41
Turn number of coil	[turn/pole]	54
Coil size	[mm]	5×6, t=1.0
Maximum current	[A]	100
Resistance	[mΩ]	84
Voltage	[V]	9
Water flow rate	[Liter/min]	1.4
Maximum water temperature rise	[℃]	10
Water pressure drop	[MPa]	0.27

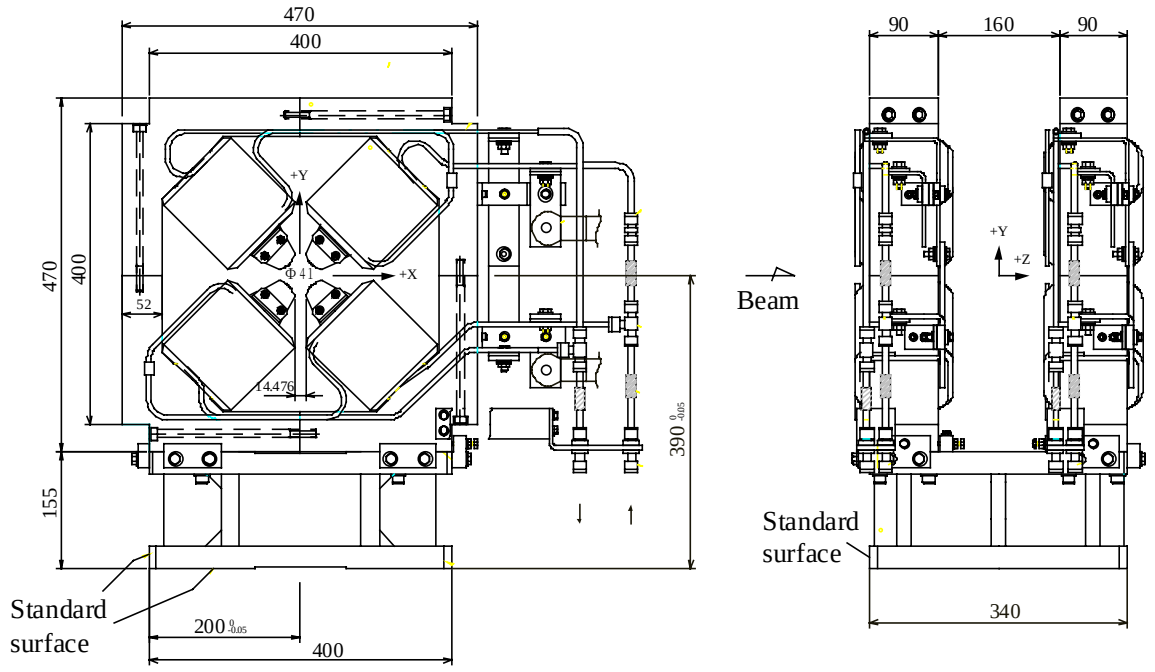

Fig. 3.1.2.4.9. Cross-sectional view of the quadrupole doublet.

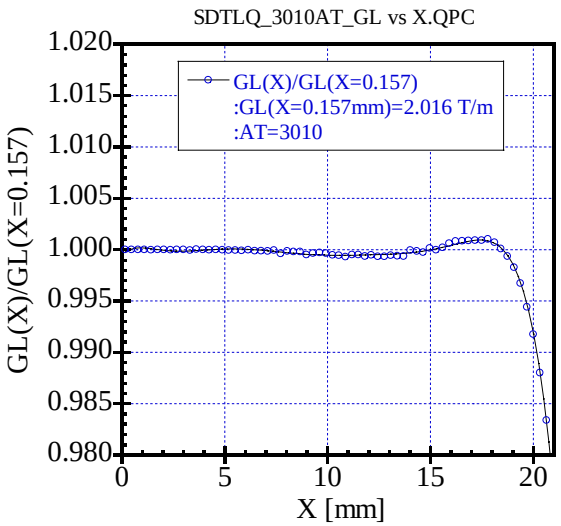

Fig. 3.1.2.4.10. Calculated radial distribution of the integrated field of the Q-magnet with the design current.

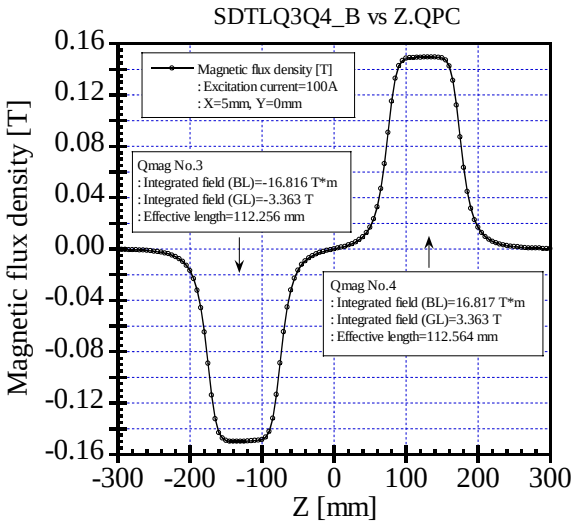

Fig. 3.1.2.4.11. Measured longitudinal distribution of the quadrupole doublet at the maximum current.

3. 1. 2. 4. 7 Pulsed-current power supply

A pulsed-current power supply with a 20 kHz switching regulator circuit (IGBT elements are used) has been developed for the magnet of the DTL. The requirements for the current supply are as follows: (1) current stability, with the flat top of the output pulse being less than 10^{-3}; (2) the duration time of the stabilized flat top should be greater than 1 msec; (3) the maximum current is 1000 A; (4) the rise time for the current pulse is 5 msec. A typical measured pattern of the output current from the supply with a dummy coil is shown in Figure 3.1.2.4.12. This shows that the stability of the current is about $5x10^{-4}$. The other requirements have also been achieved.

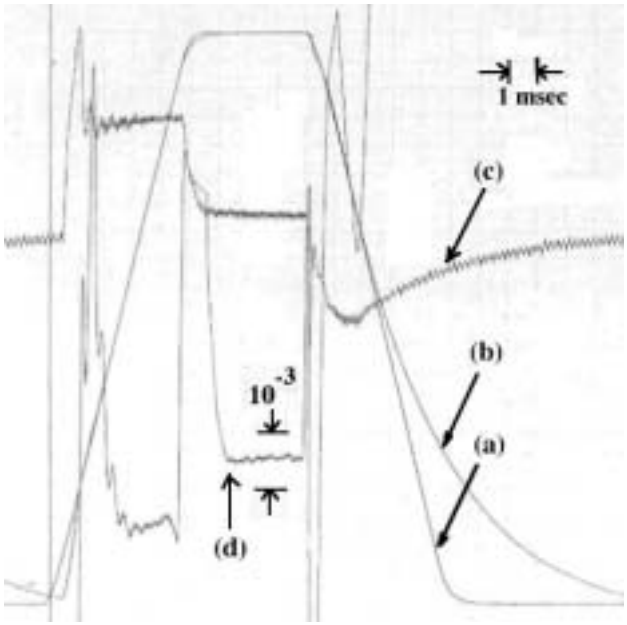

Figure 3.1.2.4.12.

Time variation in the current from the power supply. (1000A)
(a) reference pulse (input),
(b) output current,
(c) output voltage,
(d) deviation of the output current.

3. 1. 2. 4. 8 Breakdown test of the copper electrode [10,11]

An electrical breakdown test has been conducted to determine the electrical characteristics of the electroformed copper by the PR process for the DTL. Electrodes made by other processes were also tested, in order to compare their properties. The top of the electrode is hemispheric in shape, with a radius of 30mm.

Table-3.1.2.4.4. Typical first breakdown field

Materials.	The 1st breakdown field (MV/m)
EF (PR, Pure copper sulfate)	41
EF (Copper sulfate with brightener)	13
EF (Pyrophosphate)	10
OFC (Lathe finishing)	20
OFC (Electro polishing)	16
OFC (Diamond bite)	70

(EF: Electro-Forming, PR: Periodic-Reverse
OFC: Oxygen Free Cooper)

Table 3.1.2.4.4 shows typical results for the first breakdown field level. The results show that the first breakdown field for the electrode made by the PR copper electroforming is significantly higher than those of the other electrodes, except for an electrode made of OFC finished by a diamond bite. The data indicates that the surface of the electroformed copper by PR process has the most suitable properties for the accelerator cavity.

3. 1. 2. 4. 9 Input-coupler for the DTL and SDTL

Schematic views of the input coupler for the DTL and SDTL are shown in figure 3.1.2.4.13.

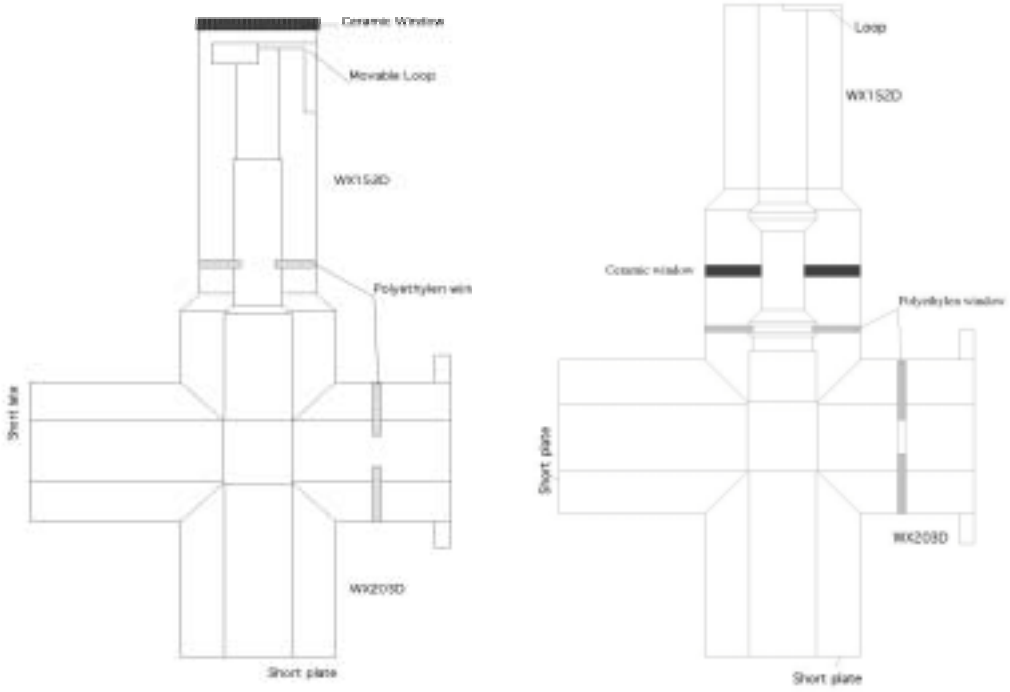

(a) Coupler for DTL (b) Coupler for SDTL

Figure 3.1.2.4.13. Cross-sectinal view of the input couplers.

Both couplers have a cross stub angle used as a line of the cooling water. The loop of the DTL coupler is movable along the inner axis of the waveguide (WX152D) by remote control in order to change the coupling between the tank and the coupler. The ceramic window for the DTL is a flat disc of which the thickness is 17 mm and made of aluminum oxide (99.7% purity). This coupler has been used for a high-power test of the DTL model tank and SDTL practical tanks. The maximum value of the rf peak power is about 530 kW. Sparking occurs around the movable loop when the input power exceeds 500 kW in peak. Thus, a modification of the design around the loop is now being carried out.

The coupler for SDTL has a coaxial disk window. The reliability of the coaxial-type disk window for the high-power rf has been proved based on a lot of experience in the TRISTAN [12] and KEKB [13] projects in KEK. The fixed loop coupler is now under construction.

3. 1. 2. 4. 10 High-power test of a model tank and SDTL

A short tank (1.4 m in length) has been made for a high-power test of the DTL components (the rf contactors for the stems and the end plates, the electroformed copper surface, a drift tube with the quadrupole magnet, tuners, and the input coupler). A schematic representation of the tank is shown in Figure 3.1.2.4.14. Only the shortest drift tube has a quadrupole magnet inside. The tank consists of the first three cells and the last four cells of the DTL. The right half of the 3rd drift tube is half of the 142nd drift tube. Thus, the position of the stem of the tube is not ideal, because the stem is located at center of the tube. Because this is likely to lead to a non-uniformity in the accelerating field (Ez) distribution, which is measured by a bead perturbation method, the non-uniformity around the 3rd drift tube, that can be seen in the data shown in Figure 3.1.2.4.15, is as expected.

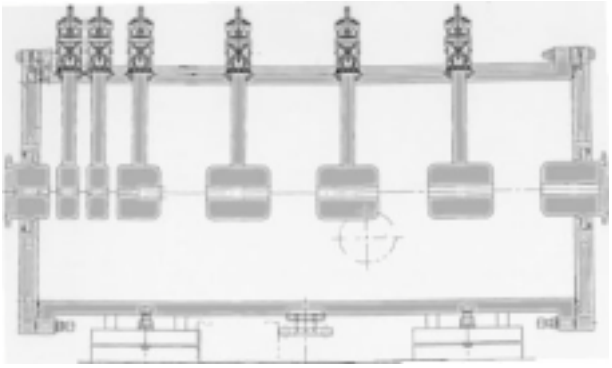

Figure 3.1.2.4.14. Schematic representation of the DTL hot model.

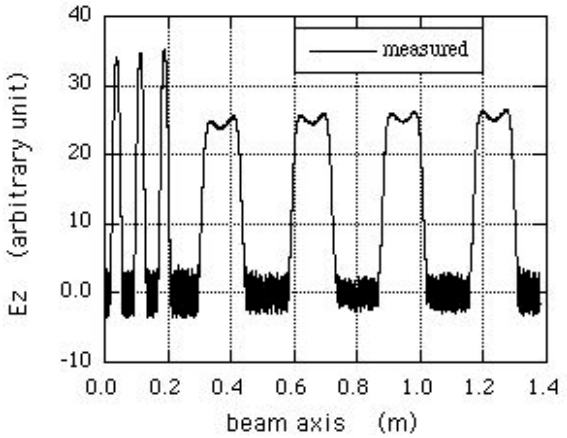

Figure 3.1.2.4.15. Electric field along the beam axis.

The measured unloaded Q-value was 46200, which is about 93% of the estimated value, and includes the effect of all components. The shunt impedance is 54.7 MΩ/m. Because the design value of the Ez is 2.5 MV/m, the required input rf-power is about 160 kW.

The first high-power conditioning was carried out at the end of April this year. Figure 3.1.2.4.16 shows the conditioning history of the tank.

The design value for the peak power was easily achieved under short-pulse (several 10 μsec in duration) operation, requiring just two days to achieve full-power operation. The high-power test was terminated when the input power level exceeded the 400 kW in peak, which is about 2.5-times the required peak power. When the end plate of the tank was opened to check the inside after the test, no trace of the discharge was observed on the inner surface of the tank, the surface of the drift

tube, or on the rf contactor for the end plate.

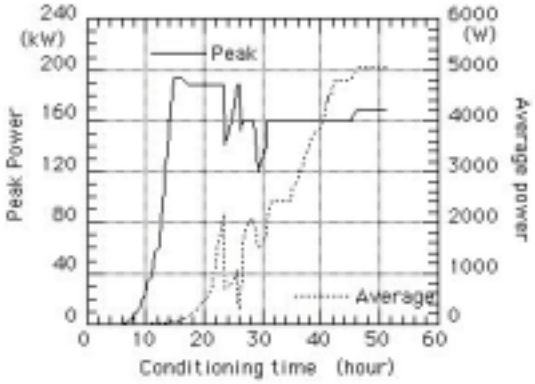

Figure 3.1.2.4.16.

Conditioning history of the DTL model tank.

The SDTL first and second tanks have also been tested by high-power rf up to about 500 kW in peak value (duty3 %). No sparking was observed in the tank.

3. 1. 2. 4. 11 Assembling of DTs for the first tank of the DTL

Drift tubes for the first tank were assembled in the tank. It took about two months. The position of the bore center of each drift tubes was measured as the distance from beam axis defined by the inner cylinder of the tank. The measured results for the horizontal plane (x-y plane) are shown in Fig. 3.1.2.4.17 (a). The difference between the design value and the assembled position for the beam axis (z axis) is also shown in Fig. 3.1.2.4.17 (b). The deviation of both position distributions are small enough to achieve the design requirement.

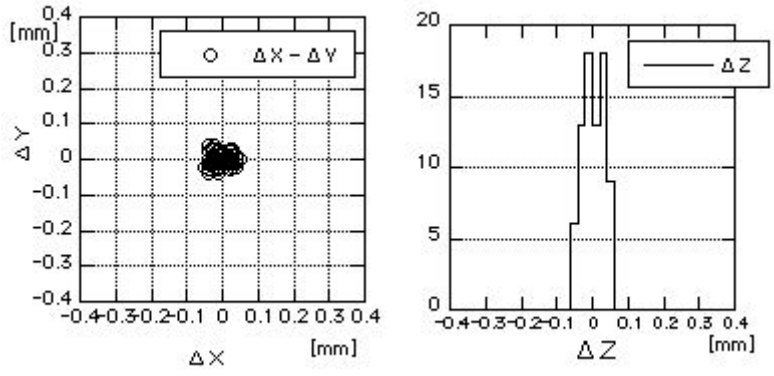

(a). (b)

Figure 3.1.2.4.17.
Distribution of the drift tubes position.
(a) Transverse position deviation from the beam axis.
(b) Longitudinal position deviation from the design value.

3. 1. 2. 4. 12 Field stability in the DTL tank during operation

It is a reasonable expectation that the accelerating-field distribution during high-

power operation differs from that measured in a low-level rf bead-perturbation measurement, since a large amount of heat dissipation in a tank during operation has some effects on the sizes of every component in a tank. The deviation of the field distribution from the design value is not large if the temperature of the tank rises uniformly by one degree during high-power operation. However, a large deformation of the field distribution can be expected if the deviation of the resonant frequency during high-power operation is compensated by a frequency tuner. Figures 3.1.2.4.18-19 show the deformed field distribution by a correction of the operating frequency with one/two tuners when a uniform temperature rise of one degree for the first DTL tank occurs. Thus, the following strategies were taken for suppressing the effects:

1. High and uniform cooling efficiency for all parts of the tank,
2. Small heat flow from the electromagnetic quadrupole magnets into the outer surface of drift tubes. Thus, the pulsed operation for the magnet power supply was chosen; the duty factor decreased by more than 60%. A hollow-conducting type coil was adopted from the viewpoint of high cooling efficiency. The efficiency of insulation for heat conduction between the magnet and the drift-tube outer surface was improved.
3. The accelerating field was stabilized by using post couplers for suppressing the deviation of the field distribution due to any perturbations,
4. Two tuners are utilized for frequency compensation.

As a result, an accelerating-field flatness within 1% during high-power operation can be expected.

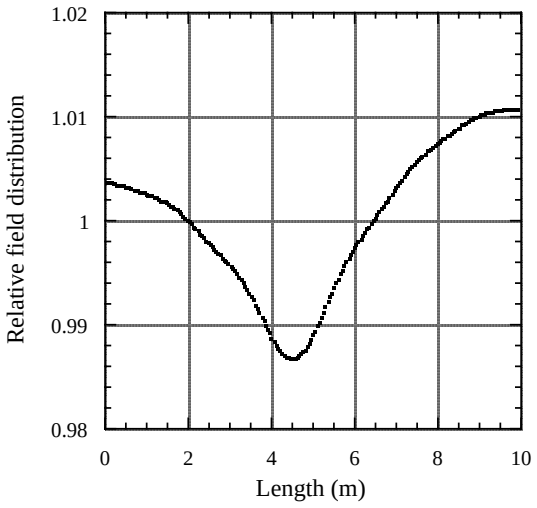

Fig. 3.1.2.4.18.
Relative field distribution along the first DTL tank. A uniform temperature rise of one degree is assumed. One tuner is used for compensating the resonant-frequency deviation. The improvement in the field stability by post-coupler is not included.

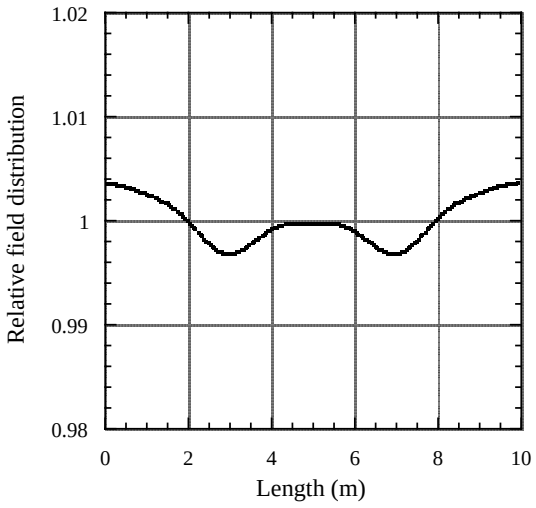

Fig. 3.1.2.4.19.
Relative field distribution along the first DTL tank. A uniform temperature rise of one degree is assumed. Two tuners are used for compensating the resonant-frequency deviation. The improvement in the field stability by post-coupler is not included.

References

[1] T. Kato, “Design of the JHP 200-MeV Proton Linear Accelerator”, KEK Report 96-17 (1997)

[2] JHF Project Office, “JHF Accelerator Design Study Report”, KEK Report 97-16, Chapter 4 (JHF-97-10) (1998)

[3] K. Tajiri et al., “Development of an electroformed copper lining for accelerator components,” Electrochimica Acta **47**, 143 (2001).

[4] K. Tajiri, et al., AESF/SFSJ Advanced Surface Technology Forum Proceedings, 145 (1998).

[5] H. Ino, et al., “Advanced Copper Lining for Accelerator Components”, Proc. of XX’th LINAC conf., California, 1015 (2000)

[6] F. Naito, et al, “Development of the 50-MeV DTL for the JAERI/KEK joint project”, Proc. of XX’th LINAC conf., California, 563 (2000).

[7] K. Yoshino, et al., "Development of the DTL Quadrupole magnet with New Electroformed Hollow Coil for the JAERI/KEK Joint Project", Proc. of XX’th LINAC conf., California, 569 (2000)

[8] K. Yoshino, et al., Proceedings of the 25th Linear Accelerator Meeting in Japan, 273 (2000), in Japanese

[9] Flat rolled magnetic steel sheets and strip of Nippon Steel Corporation, DE104, 1998.1 Edition, Nippon Steel Corporation, in Japanese

[10] Y. Saito, et al., Proc. of the 25th LINAC meeting in Japan, Himeji, Japan, 343 (2000) (in Japanese)

[11] S. Kobayashi, et al., XIX’th ISDEIV, Xi’an, China, (2000), to be published

[12] S. Isagawa, et al., Proc. IEEE Part. Accel. Conf., Washington D.C., 1934 (1987)

[13] F. Naito, et al., “The input coupler for the KEKB ARES cavity”, Proc. of 1st Asian Pacific Partcle Accel. Conf., Tsukuba, Japan, 776 (1998)